Supplementary Information

August 8, 2019

1 Materials

1,3-Diamino-2-propanol (Alfa Aesar, 97%), triethylamine (TEA) (Sigma, ≥99.5%), methanol (MeOH) (anhydrous, Sigma, 99.8%), Di-tert-butyl dicarbonate (Sigma, 99%), dichloromethane (DCM) (anhydrous, Sigma, 99.8%), dioxane (anhydrous, Sigma, 99.8%), methanesulfonyl chloride (Sigma, ≥99.7%), N,N-dimethylformamide (DMF) (anhydrous, Sigma, 99.8%), sodium azide (Sigma), tin(II) chloride dihydrate (Sigma, 98%), Fmoc chloride (Sigma, 97%), 1,8-Diazabicyclo[5.4.0]undec-7-ene (DBU) (Sigma, 98%), 1-octanethiol (Sigma, 98.5%), 2,6-di-tert-butyl-4-methylphenol (BHT) (Sigma, 99%), Alexa Fluor 647 NHS Ester (ALX)(Molecular Probes), NHS-Carboxytetramethylrhodamine (Rh)(Thermo Scientific), PA Janelia Fluor 646, SE (JF)(Tocris Bioscience), CF660C Succinimidyl Ester (CF)(Biotium, denoted CF), acetonitrile (MeCN) (anhydrous, Sigma, 99.8%), and hexadecyltrimethylammonium bromide (CTAB) (Acros Organics) were used as received. TLC plates (silica gel matrix, fluorescent indicator) were purchased from Sigma. N-isopropylacrylamide (NIPAM) (Sigma, 97%) was purified twice by recrystallization from hexane. Double distilled H_2O was filtered through 0.2 μm GHP syringe filter (Pall Laboratory) prior to use.

2 Characterization

Proton (^{1}H) NMR spectra were recorded with an Agilent 500 MHz instrument. Electrospray ionization/mass spectroscopy (ESI-MS) was carried out with a Thermo Scientific LTQ Orbitrap XL instrument. Analytical HPLC was performed on a Shimadzu Prominence system equipped with a LC-10Ai solvent delivery unit and a Photodiode Array Detector (PDA) fixed at 225 nm. A Kinetex 2.6 μm Polar C18 column was used as the stationary phase. Mobile phase consisted of a linear gradient of 100% H_2O to 50% MeOH at a flow rate of 0.5 ml/min. HPLC peak data analysis was performed with the Igor Pro 8 suite. Microgels were purified by ultracentrifugation using a Beckman Optima LE 80K. DLS was performed with a Brookhaven 90Plus instrument operating at a 90° geometry. Samples were thermally equilibrated for 20 min prior to size measurements. Hydrodynamic diameter values are given as the intensity based average of 4 consecutive measurements. For the determination of crosslinker@rhodamine conjugates consumption rate, UV-Vis spectra of aliquot supernatants after ultracentrifugation were obtained on a Perkin-Elmer Lambda 650 spectrophotometer. Reduced absorbance values were derived after subtracting residual absorbance and normalizing with the absorbance of the unreacted monomer solution.

3 Acrylamide crosslinker synthesis

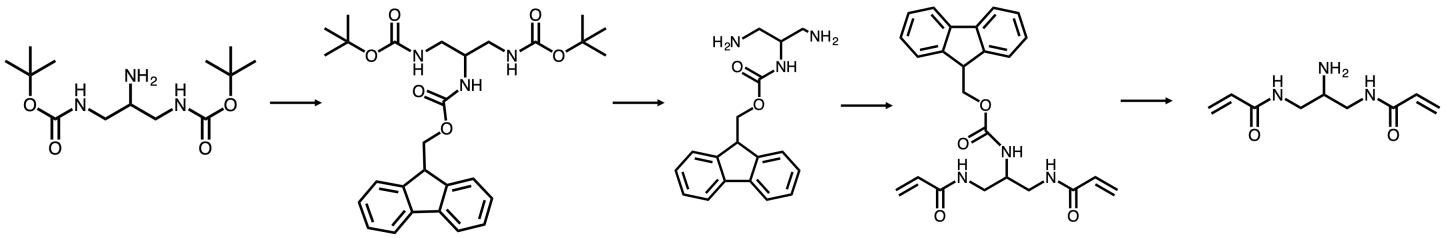

Figure 1: Aminated acrylamide crosslinker synthesis overview

3.1 Di-tert-butyl (2-aminopropane-1,3-diyl)dicarbamate (DAP-$(BocNH)_2$-NH_2)

Synthesized according to [2]. ESI-MS (DAP-$(BocNH)_2$-NH_2): 290.2076 [M+H^+]. See Figure 2 for NMR.

3.2 (9H-fluoren-9-yl)methyl di-tert-butyl propane-1,2,3-triyltricarbamate (DAP-$(NHBoc)_2$-NHFmoc)

DAP-$(BocNH)_2$-NH_2 (1 g, 3.46 mmol) was suspended in 10 ml saturated NaHCO3 in an ice-water bath, after which Fmoc-Cl (894 mg, 3.46 mmol) dissolved in 10 ml dioxane was slowly added. The resulting slurry was vigorously stirred, diluted further using 20 ml of the solvent mixture (still at 0°C) and left to react overnight after slowly returning at room temperature. The crude product was concentrated at reduced pressure and washed twice with DCM. The organic phase was washed with brine and dried over Na_2SO_4. The solvent was evaporated under vacuum to afford a white solid which was adequately pure for use in the next step. Yield: 72% ESI-MS (DAP-$(BocNH)_2$-NHFmoc): 356.1615 [M+Na+H^+] See Figure 3 for NMR.

3.3 2-((((9H-fluoren-9-yl)methoxy)carbonyl)amino)propane-1,3-diaminium chloride (DAP-NHFmoc)

DAP-Boc-NHFmoc (1g, 1.76 mmol) was suspended in 31.2 ml EtOAc and 14.6 ml of 6M HCl was added. The reaction was left to proceed overnight followed by evaporation of solvents at reduced pressure. The crude slurry was resuspended in EtOAc and centrifuged to obtain the diamine hydrochloric salt as a powdery white solid which was purified by 4 cycles of resuspension/centrifugation using ethyl ether. Yield: 84% ESI-MS (DAP-NHFmoc): 312.1711 [M+H^+] See Figure 4 for NMR.

3.4 (9H-fluoren-9-yl)methyl (1,3-diacrylamidopropan-2-yl)carbamate (BA-NHFmoc)

DAP-NHFmoc (350 mg, 0.91 mmol), 1.27 ml TEA (9.1 mmol) and 10 ml DCM were combined in a round bottom flask under Ar at 0°C. Acryloyl chloride (162 μl, 2 mmol) was added dropwise through a septum and the reaction was left to return slowly at room temperature. The reaction was left to proceed for 2 hours followed by solvent evaporation, extraction with DCM/0.1M HCl and 2x back-extraction of the aqueous phase with DCM. The combined organic phase was washed with brine, dried over Na_2SO_4 and condensed. The crude product was purified with silica flash gel chromatography using 92% DCM/MeOH as the eluent. Evaporation at reduced pressure followed by high vacuum drying yields the pure product as a white solid. Yield: 8%. ESI-MS (BA-NHFmoc): 420.1925 [M+H^+] See Figure 5 for NMR.

3.5 N,N'-(2-aminopropane-1,3-diyl)diacrylamide (BA-NH_2)

A facile Fmoc deprotection protocol was adopted according to [4]. BA-NHFmoc (24 mg, 0.057 mmol) was treated with 10x eq. of octanethiol (0.57 mmol, 84 mg) and 1.5x eq. of DBU (0.0792 mmol, 12.5 mg) in 2 ml of anhydrous THF. Complete disappearance of the starting material after 1h was verified by TLC. After removal of THF in reduced pressure the crude was purified by repetitive washing with diethyl ether until the dibenzofulvene byproduct was not detectable in TLC. The pure BA-NH2 was finally precipitated with 1M HCl in ethyl acetate and diethyl ether in the presence of trace amounts of BHT as a light brown oil. Yield: 95%. ESI-MS (BA-NH_2): 198.1244 [M+H^+] See Figure 6 for NMR.

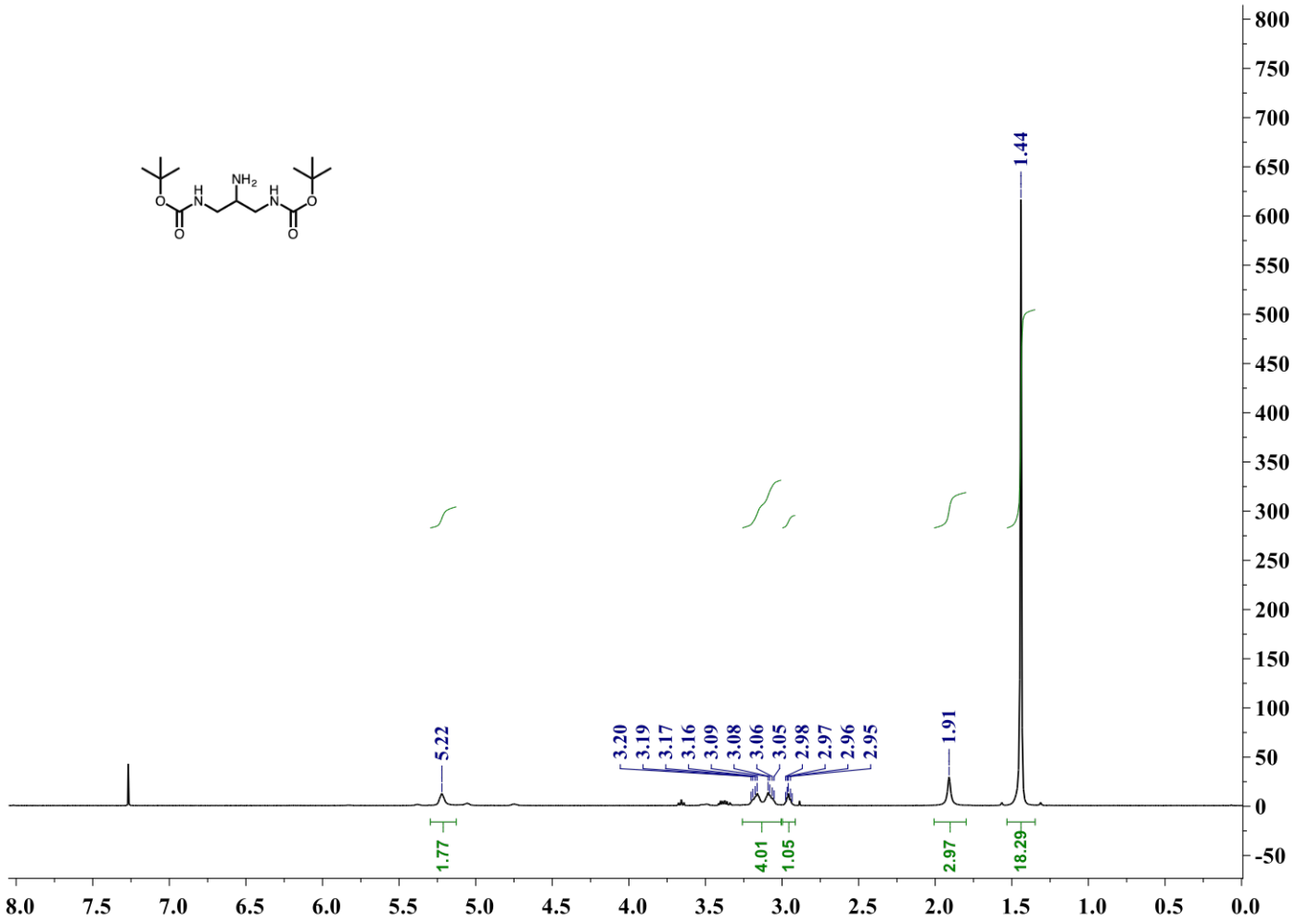

Figure 2: NMR DAP-$(BocNH)_2$-NH_2

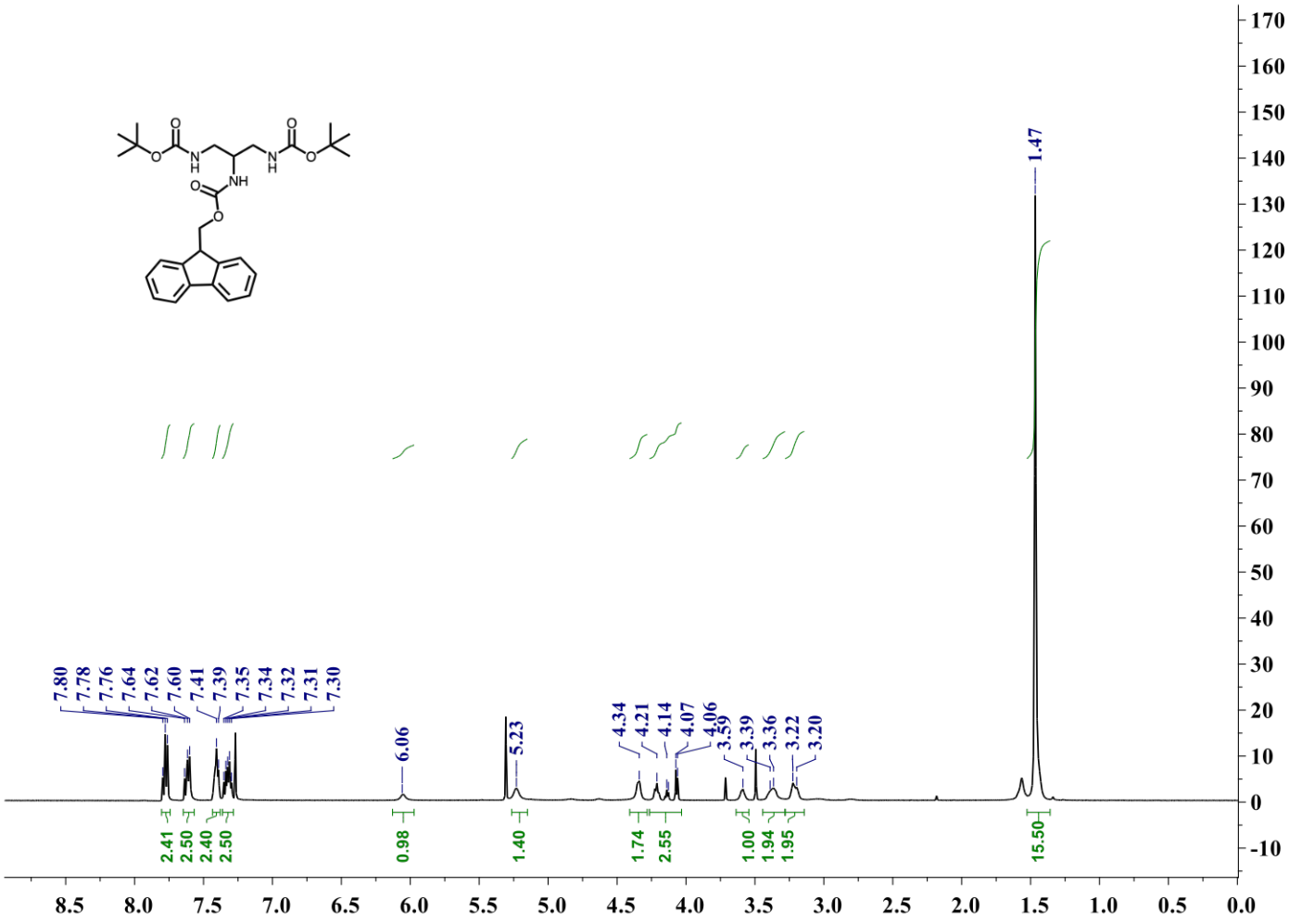

Figure 3: NMR DAP-$(NHBoc)_2$-NHFmoc

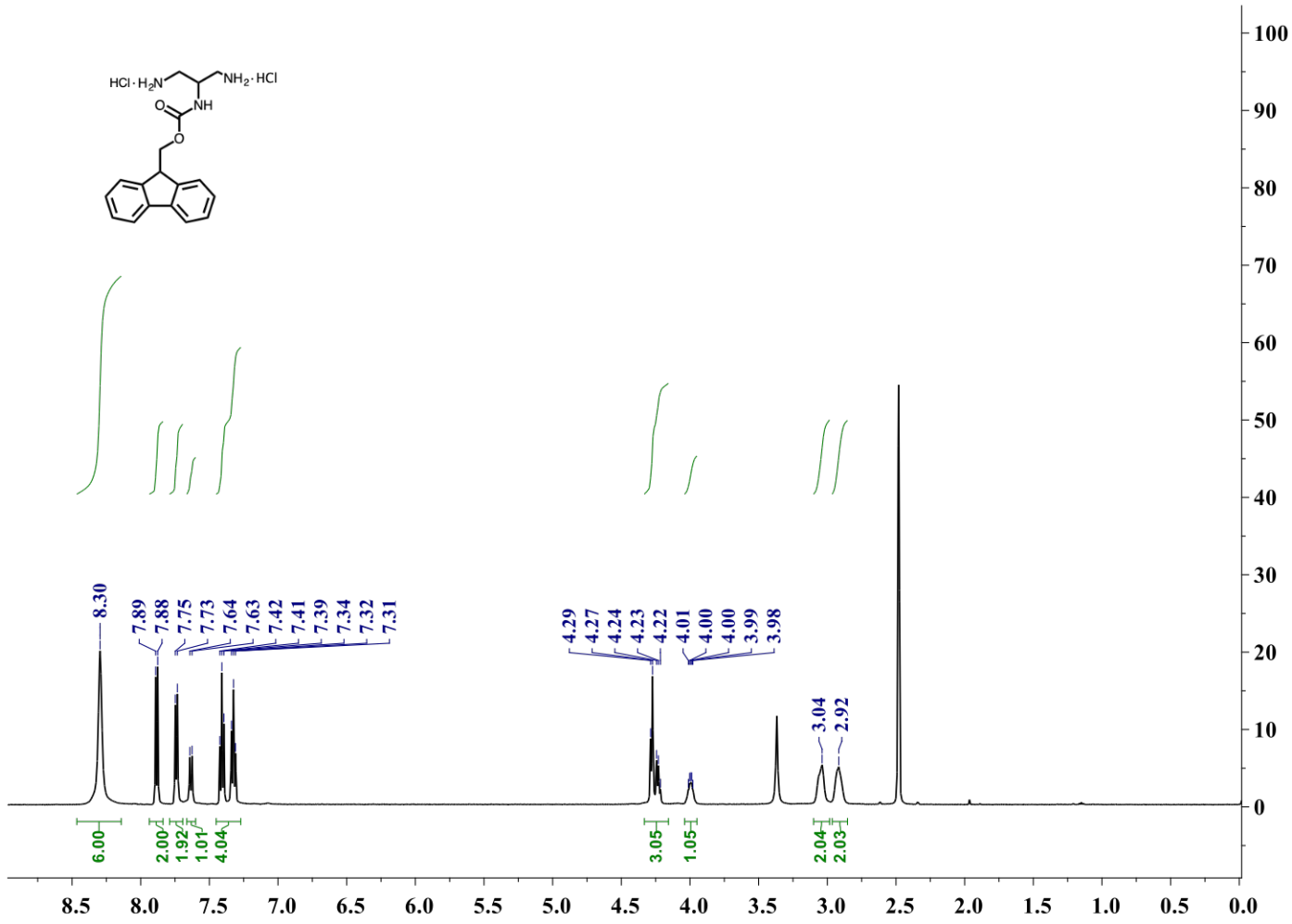

Figure 4: NMR DAP-NHFmoc

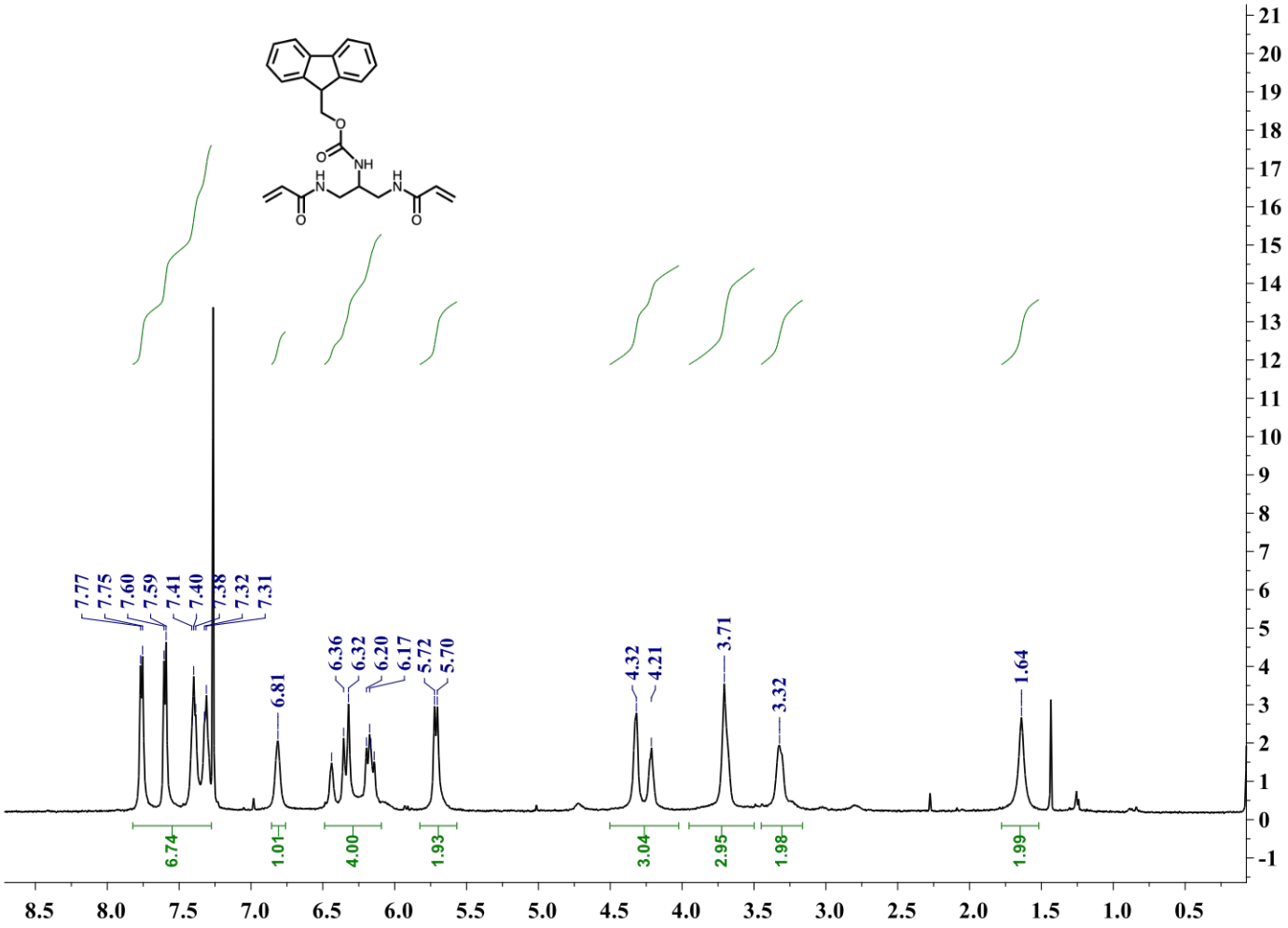

Figure 5: NMR BA-NHFmoc

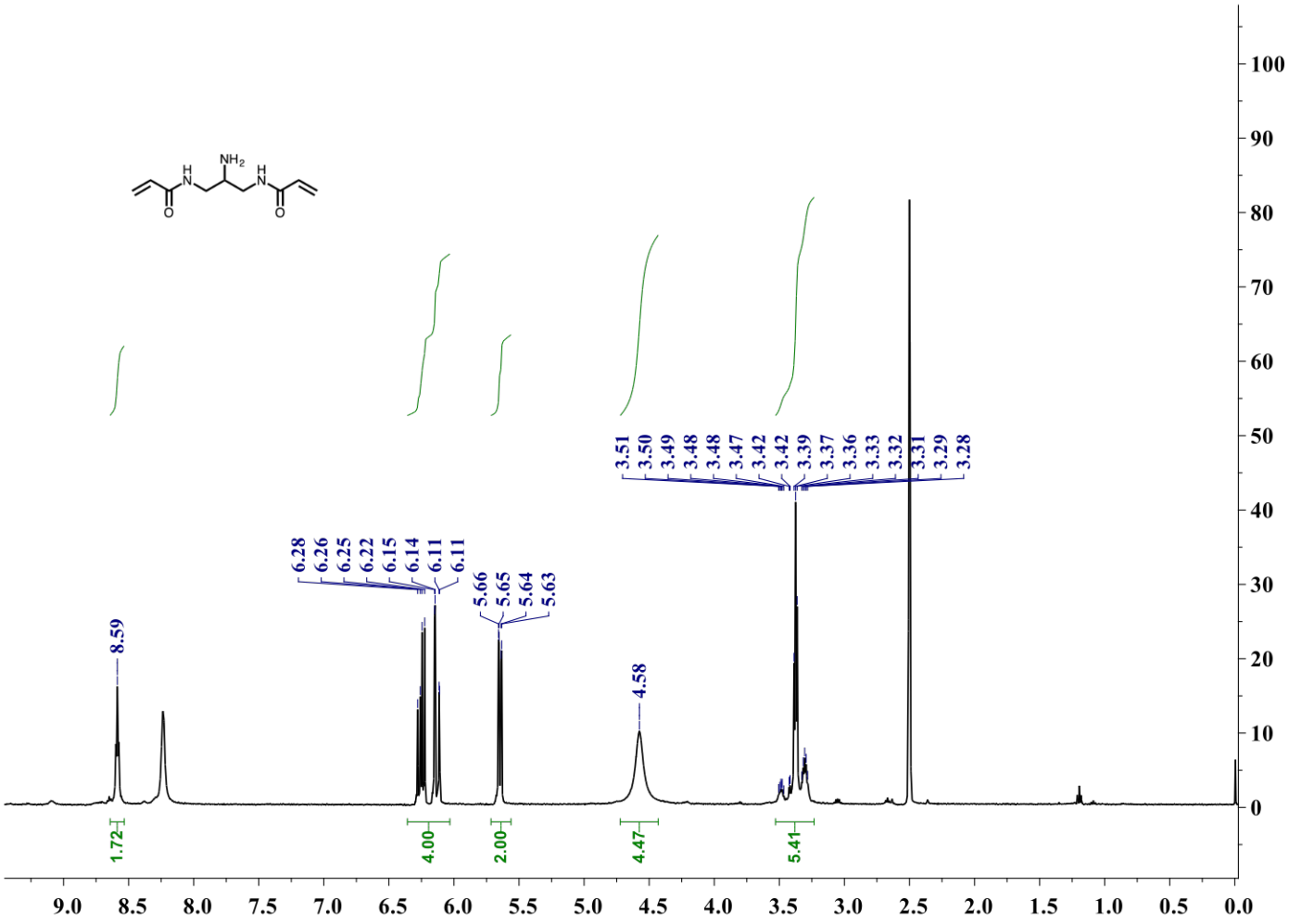

Figure 6: NMR BA-NH_2

4 Crosslinker@dye conjugates synthesis [3]

Stock solutions (1mg/ml) for each amine reactive dye were prepared using dry DMF. In a typical run for the preparation of BA@ALX, 0.2 ml of Alexa 647 NHS (0.2 mg, 1 eq.), BA-NH_2 (0.076 mg, 2.5eq.) and 20 μl TEA were combined into an 1 dram vial under Ar and left to react overnight. The reaction was condensed under reduced pressure after which H2O was added for the preparation of crosslinker-dye conjugate stocks at a final concentration of 0.2 mg/ml. The same procedure was followed for the preparation of the remaining crosslinker@dye conjugate pairs (BMA@ALX, BA@Rh, BMA@Rh, BA@CF, BMA@CF, BA@JF and BMA@JF).

5 Dynamic Light Scattering versus temperature for additional Cyanine and Rhodamine based dyes

Figure 7 shows representative examples of the impact of attaching cyanine (JF) and rhodamine (CF) dye molecules to BMA and BA crosslinker variants on microgel radius and swelling ratio.

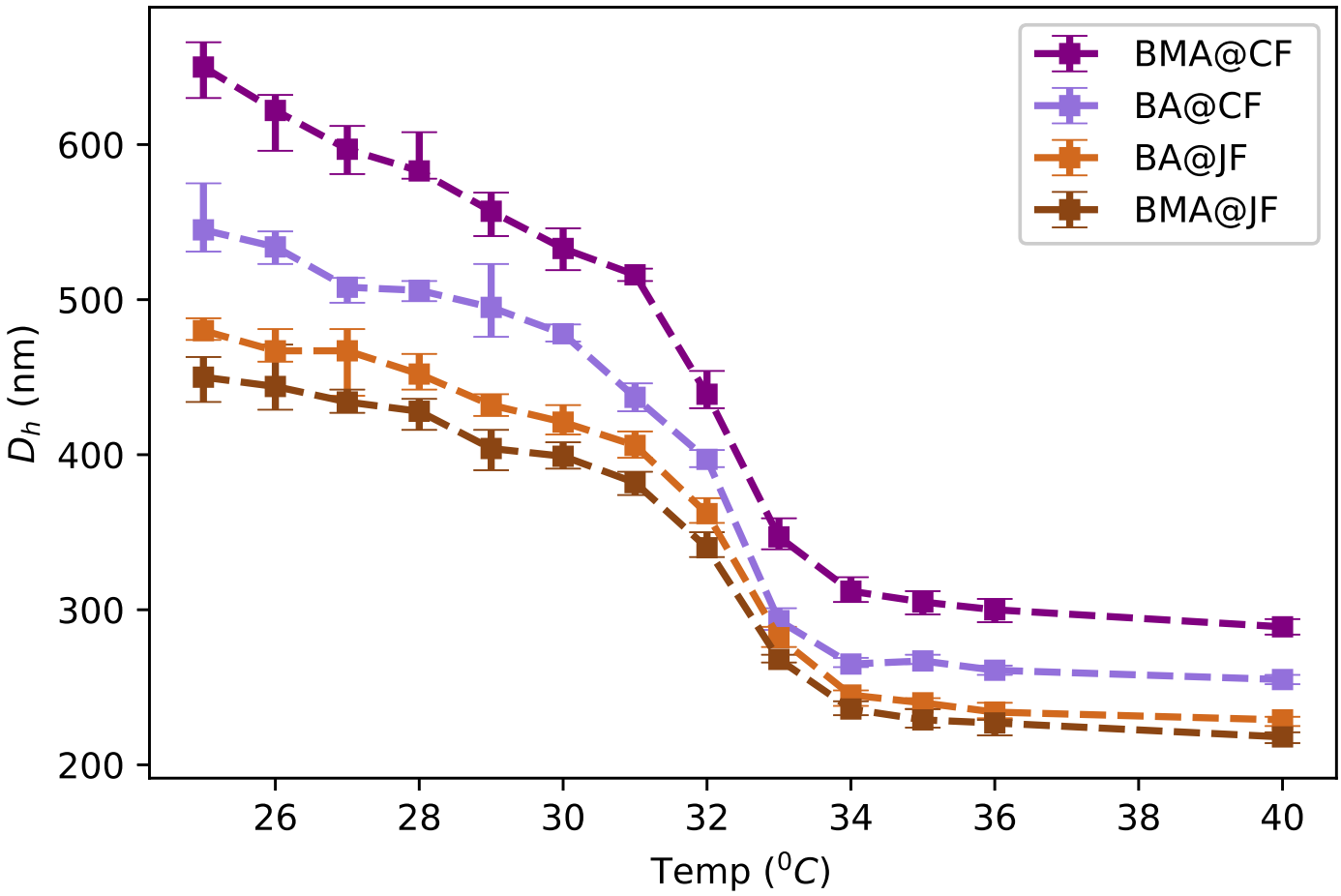

Figure 7: Hydrodynamic radii measured by dynamic light scattering versus temperature for microgels containing trace quantities of methacrylamide and acrylamide variants of dye tagged crosslinkers

6 Determination of rate constants via Price-Alfrey scheme:

The main text describes the determination of rate constants ($k_{13}, k_{23}, k_{31}, k_{32}, k_{33}$) for the reactions involving crosspropagation and homopropagation of the dye tagged cross-linker species by reducing them into three parameters (Q_3, e_3 and k_{33}) via the the Price-Alfrey scheme[1]. This is done as follows:

$$\frac{k_{22}}{k_{23}} = \frac{Q_2}{Q_3}\, e^{-e_2(e_2-e_3)} \quad (1) \qquad \frac{k_{11}}{k_{13}} = \frac{Q_1}{Q_3}\, e^{-e_1(e_1-e_3)} \quad (2)$$

$$\frac{k_{32}}{k_{33}} = \frac{Q_2}{Q_3}\, e^{-e_3(e_2-e_3)} \quad (3) \qquad \frac{k_{31}}{k_{33}} = \frac{Q_1}{Q_3}\, e^{-e_3(e_1-e_3)} \quad (4)$$

The three unknown parameters are then determined from two methods. The first involves a direct implementation (constant R_{total}) of a terminal co-polymerization model while the second applies a modified form of the model (time varying R_{total}), in which the steady state constraint is released (refer to main text for details). The maximum likelihood estimates, error estimates and co-variances of the parameters for the two models are obtained from a Bayesian regression model described in the main text. The results are depicted in figures 8 and 9 of this ESI document. The diagonal plots in the figures depict histograms of the sampled parameters from which the mean and the standard deviations are obtained. The off-diagonal plots depict projections of the distributions of the best fit values along two axes in parameter space and further provide a visualization of the co-variances between the best fit parameters along the two axes. The lack of co-variance in the off-diagonal plots confirms the reliability of the best fit parameter estimates. The maximum likelihood and error estimates for the both models are reported table 1 in the main text. The corresponding probability distribution functions used for the maximum likelihood estimates of the parameters and cumulative distribution functions used for the error estimates are reported in figures 11 and 12.

7 Determination of independent and unconstrained rate constants:

For comparison the rate constants were determined while treating the five rate constants as independent and unconstrained fit parameters. The maximum likelihood and error estimates along with the co-variances of the parameters from this method are obtained from the application of a Bayesian regression model, the results of which are shown in figure 10. The estimated values of the rate constants are reported in table 1.The corresponding probability distribution functions used for the maximum likelihood estimates of the parameters and cumulative distribution functions used for the error estimates are reported in figure 13. As compared to the rate constants determined using the steady state Price-Alfrey scheme, the root mean square error (rmse) using the best fit parameters improved marginally from 0.031 to 0.029. An improvement in rmse is expected when the number of fit parameters is increased. However, several of the resultant rate constants became ill-defined, with large 70 percent confidence intervals relative to the mean.

Table 1: Rate constants for BMA@Rh calculated using a terminal copolymerization model. All units are in $[L.mol^{-1}.s^{-1}]$. Parameters are reported as Mean [+Upper Error, -Lower Error Bound]

Parameter	Independent treatment
k_{13}	6.90×10^5 $[+3.60 \times 10^5, -9.0 \times 10^4]$
k_{23}	35 [+715, −32]
k_{31}	25 [+5, −10]
k_{32}	165 [+385, −115]
k_{33}	9 [+41, −5]
$rmse$	0.029

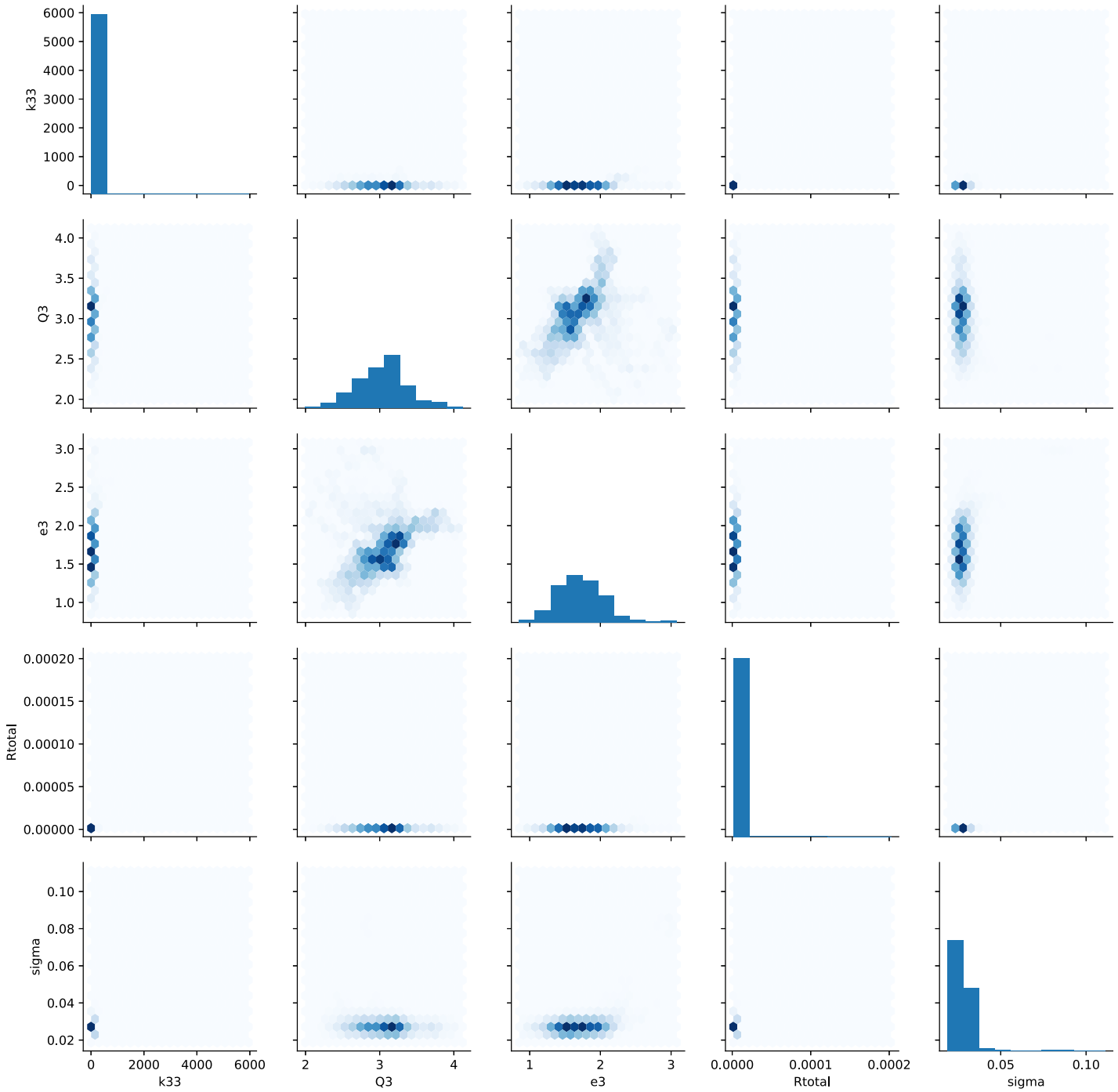

Figure 8: Sampled probability distributions of each parameter and their co-variances obtained from Price-Alfrey scheme (constant R_{total})

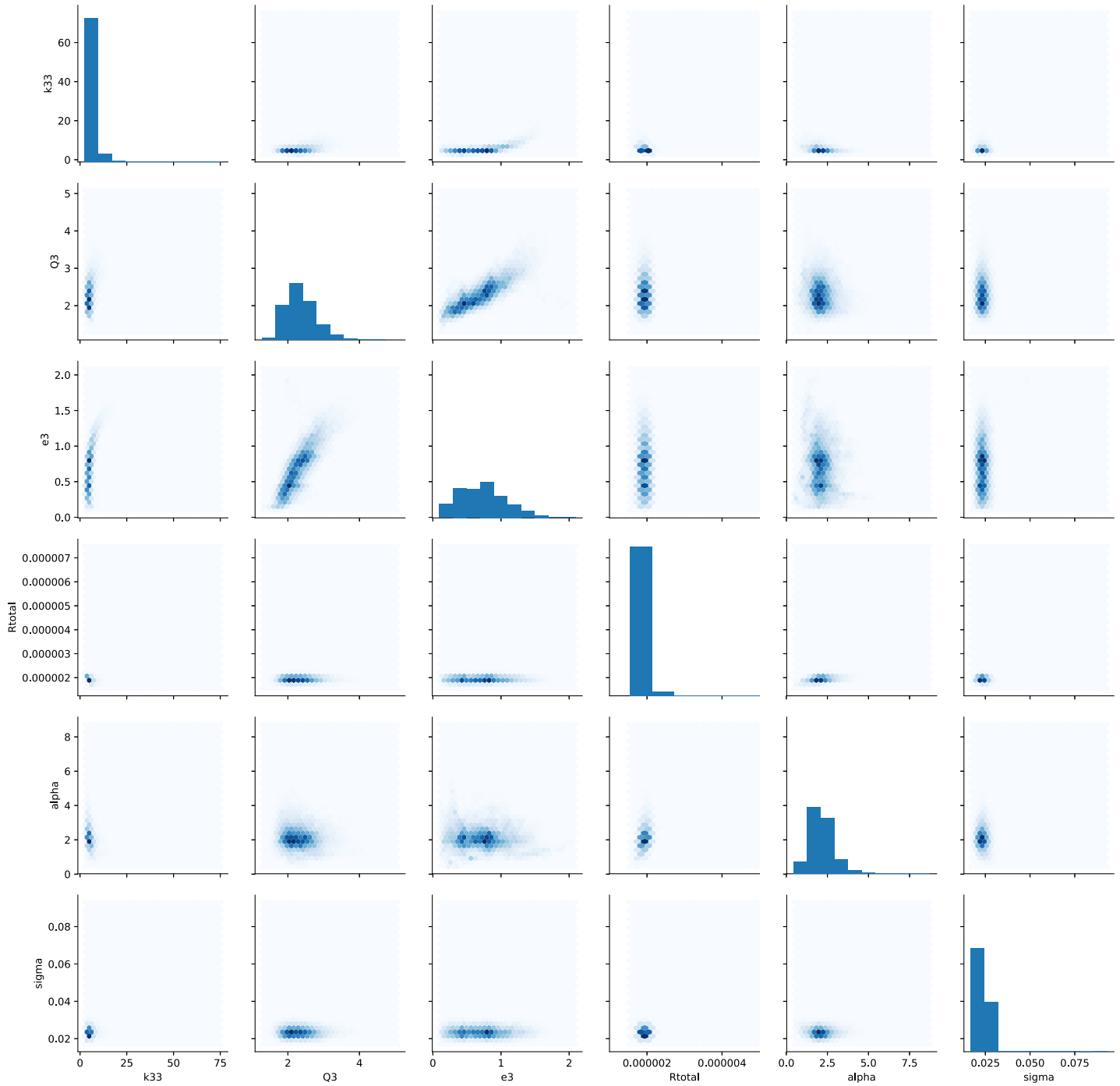

Figure 9: Sampled probability distributions of each parameter and their co-variances obtained using the non-steady state approximation in the Price-Alfrey scheme (time varying R_{total})

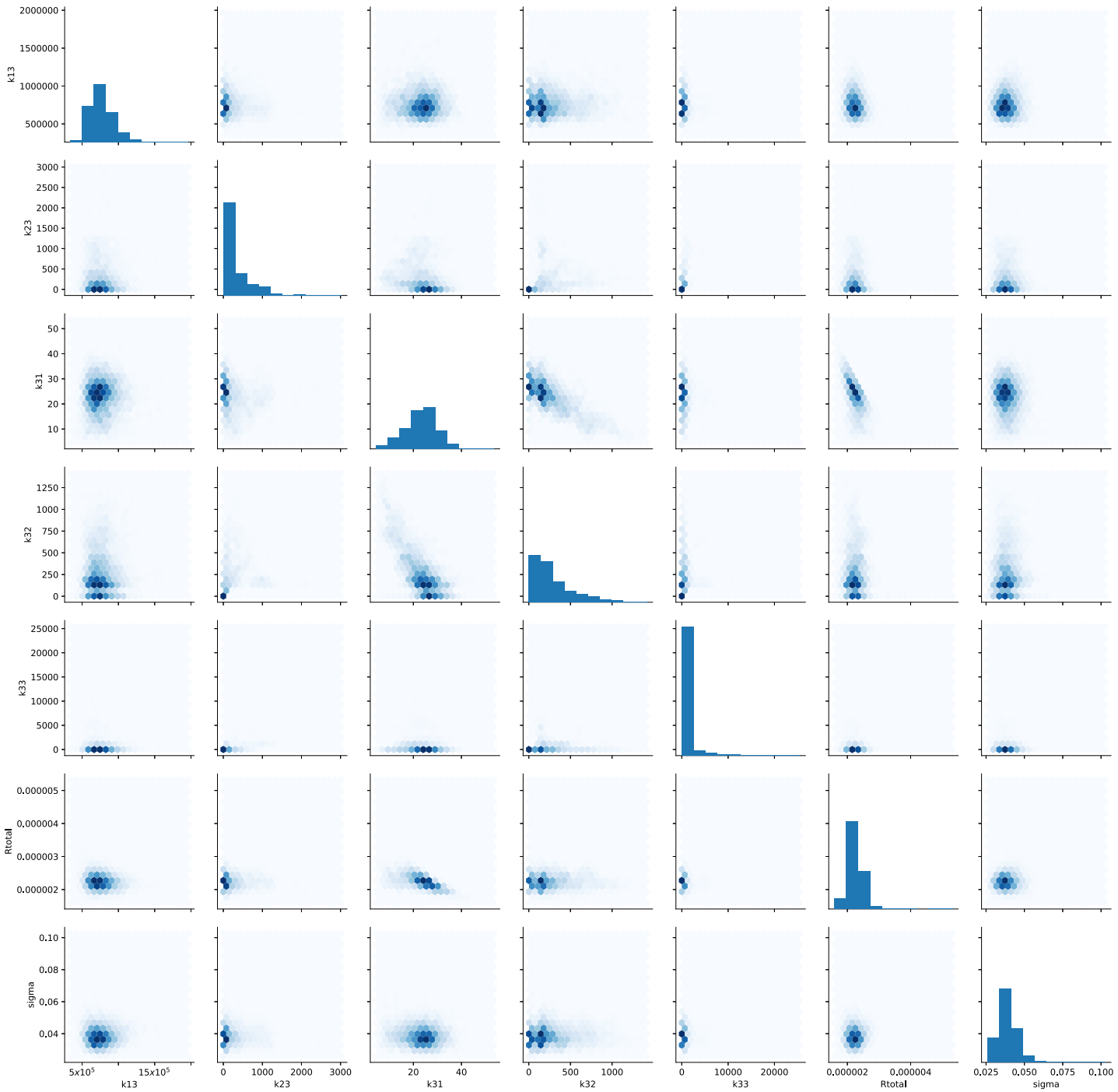

Figure 10: Sampled probability distributions of each parameter and their co-variances obtained from treating the rate constants as five independent parameters

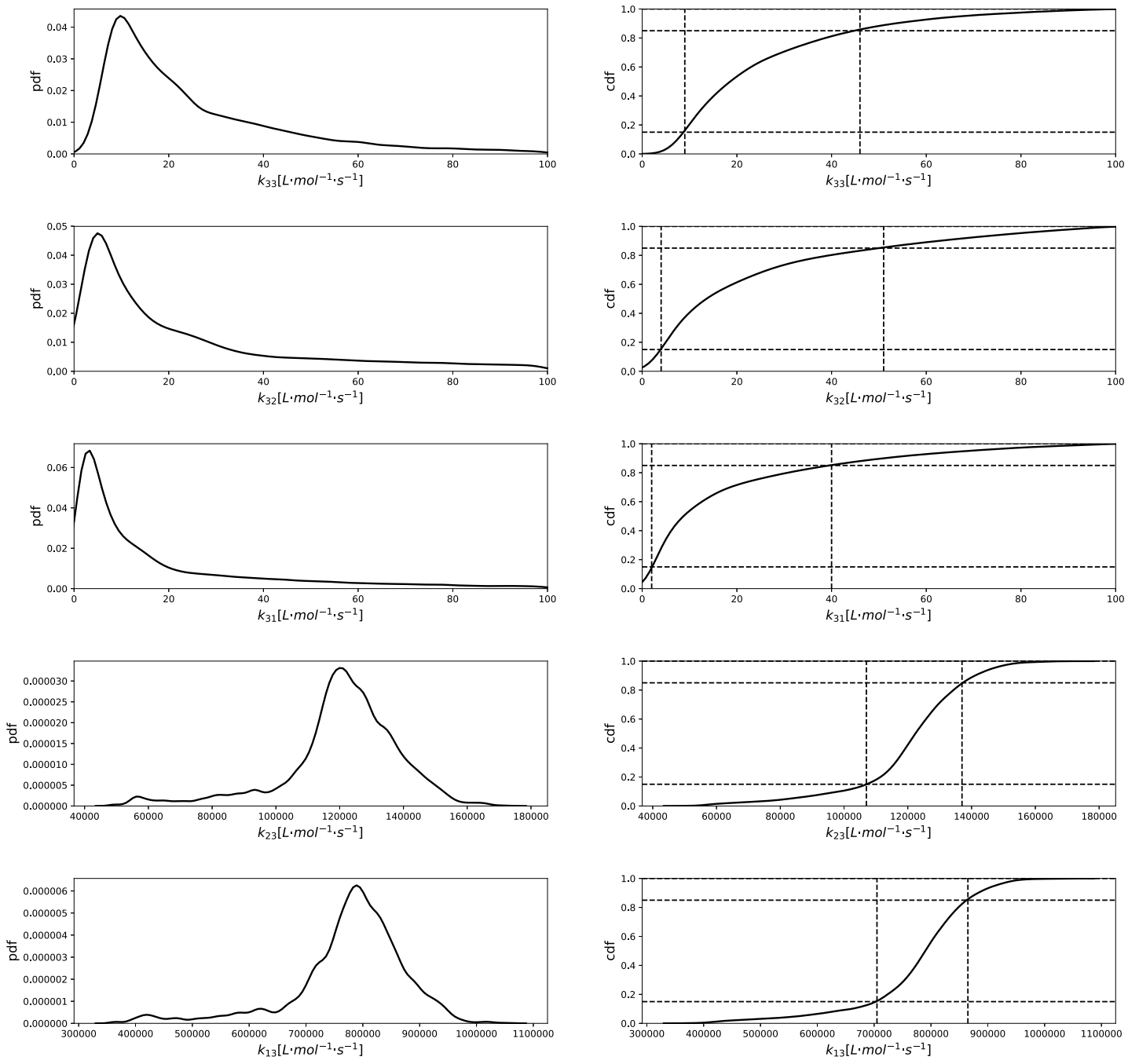

Figure 11: Probability distribution function (pdf) and the corresponding cumulative distribution function (cdf) of each sampled parameter distribution obtained using the Price-Alfrey scheme (constant R_{total}). Dotted lines indicate the confidence interval in the cdf used to in the error estimate

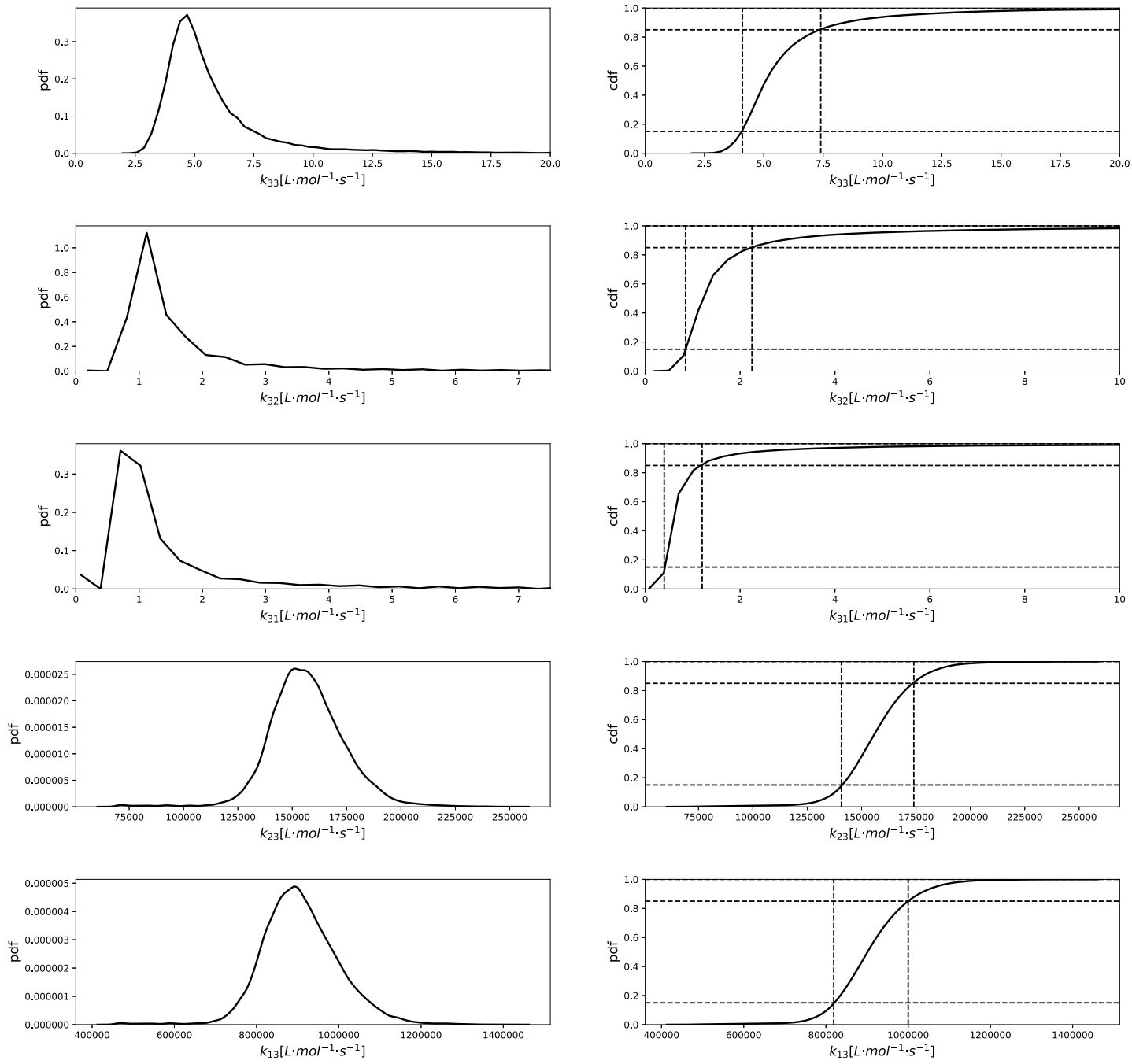

Figure 12: Probability distribution function (pdf) and the corresponding cumulative distribution function (cdf) of each sampled parameter distribution obtained using the non-steady state approximation in the Price-Alfrey scheme (time varying R_{total}). Dotted lines indicate the confidence interval in the cdf used to in the error estimate

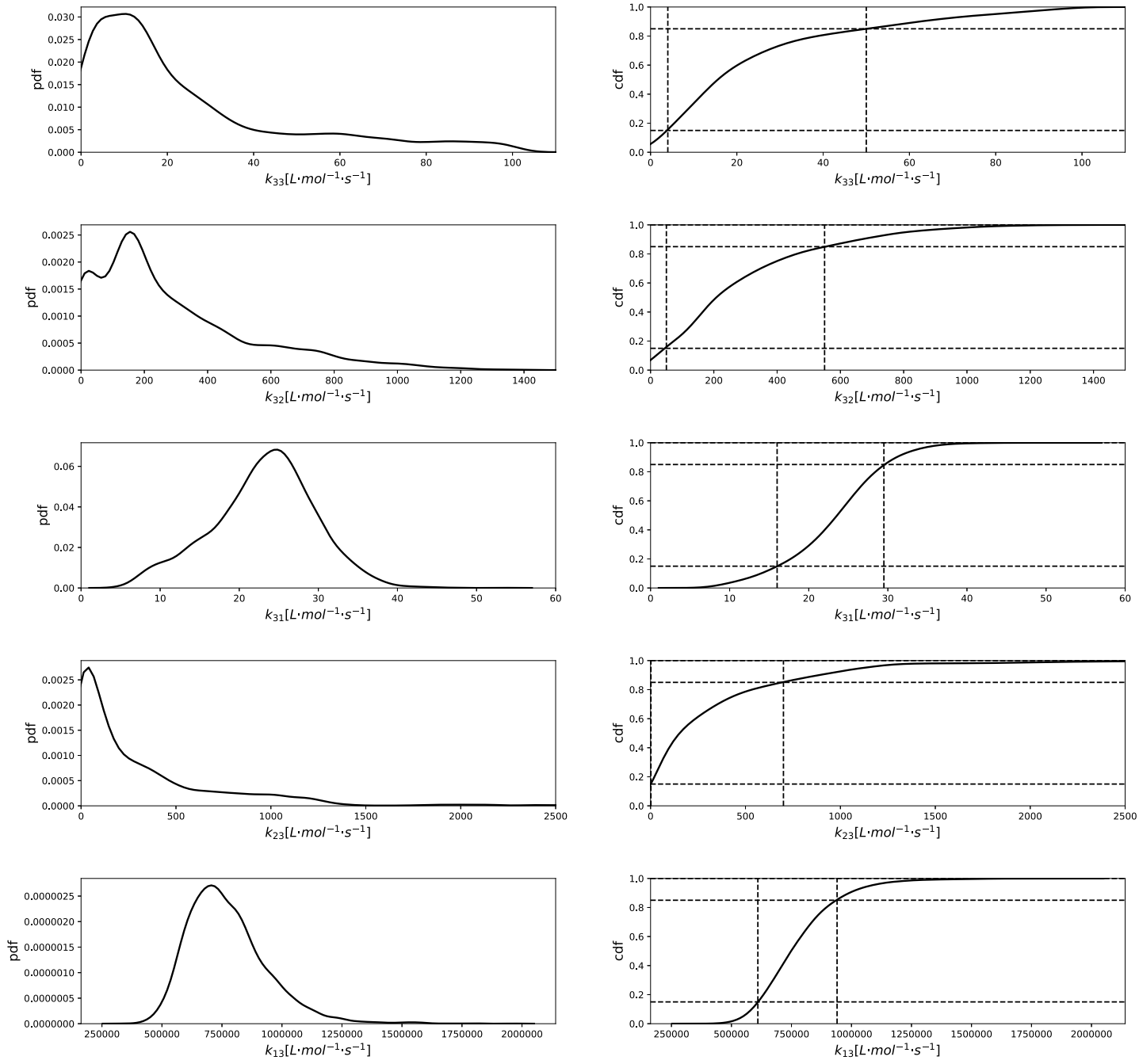

Figure 13: Probability distribution function (pdf) and the corresponding cumulative distribution function (cdf) of each sampled parameter distribution obtained from treating the rate constants as independent. Dotted lines indicate the confidence interval in the cdf used to in the error estimate

References

[1] Turner Alfrey Jr. and Charles C. Price. Relative reactivities in vinyl copolymerization. *Journal of Polymer Science*, 2(1):101–106, 1947.

[2] E. Benoist, A. Loussouarn, P. Remaud, J-F. Chatal, and J-F. Gestin. Convenient and simplified approaches to n-monoprotected triaminopropane derivatives: Key intermediates for bifunctional chelating agent synthesis. *Synthesis*, 1998(08):1113–1118, 1998.

[3] A. A. Karanastasis, Y. Zhang, G. S. Kenath, M. D. Lessard, J. Bewersdorf, and C. K. Ullal. 3D mapping of nanoscale crosslink heterogeneities in microgels. *Mater. Horiz.*, 5:1130–1136, 2018.

[4] J. E. Sheppeck, H. Kar, and H. Hong. A convenient and scaleable procedure for removing the fmoc group in solution. *Tetrahedron Letters*, 41(28):5329–5333, 2000.